photonics

IMPACT FACTOR 2.1

CITESCORE 2.6

Article

Nonlinear-Optical Processing of OAM Light States in a Few-Mode Fiber

Cheng Guo, Afshin Shamsshooli, Francesca Parmigiani, Xiaoying Li and Michael Vasilyev

Special Issue

Progress in OAM Beams: Recent Innovations and Future Perspectives

Edited by

Dr. Eric G. Johnson and Dr. Miranda Van Iersel

MDPI

https://doi.org/10.3390/photonics12030233

photonics

MDPI

Article

Nonlinear-Optical Processing of OAM Light States in a Few-Mode Fiber

Cheng Guo [1], Afshin Shamsshooli [1], Francesca Parmigiani [2], Xiaoying Li [3] and Michael Vasilyev [1,*]

[1] Department of Electrical Engineering, University of Texas at Arlington, Arlington, TX 76019, USA
[2] Microsoft Research, Cambridge CB4 0AB, UK
[3] Key Laboratory of Opto-Electronic Information Technical Science of Ministry of Education, College of Precision Instruments and Opto-Electronics Engineering, Tianjin University, Tianjin 300072, China
* Correspondence: vasilyev@uta.edu

Abstract: Utilizing the phase-matching conditions of inter-modal four-wave mixing in an elliptical-core few-mode fiber supporting three non-degenerate modes, we experimentally demonstrate schemes for generating orbital-angular-momentum (OAM)-entangled photon pairs with high mode purity and for achieving highly mode-selective frequency conversion of beams in OAM-compatible (LP_{11a}, LP_{11b}) mode basis. These techniques expand the toolbox for using OAM modes in both classical and quantum communications and information processing.

Keywords: nonlinear fiber optics; intermodal four-wave mixing; optical parametric amplification; wavelength conversion; orbital angular momentum; quantum information processing

1. Introduction

Spatial modes (e.g., those of multimode fibers and waveguides) represent an important degree of freedom for increasing the capacity of both classical and quantum communications [1,2]. For both communication types, using different spatial modes as separate communication channels yields the capacity increase proportional to the number of modes. Alternatively, in the quantum case, the use of entanglement in multiple degrees of freedom (e.g., in polarization [3], frequency [4], time-bin [5,6], and spatial modes) may enable new communication and networking protocols relying on quantum information encoding in high-dimensional Hilbert space. While polarization, frequency, and time-bin entanglement generation has already been implemented in an integrated platform compatible with low-loss transport over optical fiber, the spatial entanglement still relies on bulk-crystal-based setups, e.g., spatially- or orbital-angular-momentum- (OAM) entangled photons have been generated in crystal platforms and transported over hollow-core photonic crystal fiber [7], a few-mode fiber (FMF) [8], and vortex fiber [9]. On the other hand, the FMF itself has been recently gaining traction as a platform for nonlinear-optical signal processing based on inter-modal four-wave mixing (IM-FWM) [10]. This is because the mature and flexible fiber design and manufacturing employed in making the FMF provide wide options for mode- and dispersion-engineering, as well as for an excellent mode match to the FMFs used in low-loss transmission links. IM-FWM in FMF has been used for tunable wavelength conversion [11–13] and correlated photon-pair generation [14–16], but no attempts of spatial-mode entanglement have been made yet. We have recently described a novel scheme for the generation of spatial-mode-entangled photon pairs in LP_{01} and LP_{11} modes directly in the FMF using a combination of two IM-FWM processes [17–19]. In the present

check for updates

Received: 31 December 2024
Revised: 19 February 2025
Accepted: 1 March 2025
Published: 4 March 2025

Citation: Guo, C.; Shamsshooli, A.; Parmigiani, F.; Li, X.; Vasilyev, M. Nonlinear-Optical Processing of OAM Light States in a Few-Mode Fiber. *Photonics* **2025**, *12*, 233. https://doi.org/10.3390/photonics12030233

paper, we extend this scheme to LP_{11a} and LP_{11b} modes, which can enable the generation of OAM-entangled photon pairs. A brief preliminary report on this work was given in a conference paper [20].

Another requirement for communications with multiple spatial modes is the availability of dynamically reconfigurable spatial-mode demultiplexers. In classical communications, such a demultiplexer, in addition to separating individual spatial channels, can also undo the mode mixing taking place in the transmission fiber [21], which relaxes the requirements for electronic processing of the received signals. In quantum communications using high-dimensional Hilbert space for encoding, the same demultiplexer enables projective measurements that can alternate between mutually unbiased spatial-mode bases. In either case, the low loss and low crosstalk of the demultiplexer are important. Previously, we have proposed [22] and experimentally demonstrated such a demultiplexer in a two-mode $LiNbO_3$ waveguide [23,24], where, by adjusting the spatial profile of a 1560-nm pump wave, we could selectively upconvert either mode TM_{00} or mode TM_{01}, or any superposition of these two modes of a 1540-nm signal to TM_{01} mode at 775 nm, for both classical [23] and single-photon-level [24] signals. More recently, we have demonstrated a scheme of similar functionality (mode demultiplexing by mode-selective frequency conversion) in a $\chi^{(3)}$ nonlinear medium by using a combination of two IM-FWM processes in an FMF [25–30]. Compared to the $LiNbO_3$ platform, nonlinear FMFs can offer wider design options for mode- and dispersion-engineering and better mode match to the FMFs used in transmission links. The IM-FMF allows for the dynamic reconfigurability of the demultiplexer's mode basis by controlling the spatial modes and wavelengths of the pumps and taking advantage of mode-selective phase-matching conditions of IM-FMF. Our results [25] have shown good crosstalk performance (mode selectivity) for each of the two required IM-FWM processes individually. In [26,27], we implemented both processes simultaneously and demonstrated their combined ability to handle any superposition of LP_{01} and LP_{11a} modes in the two-mode signal space. In this paper, expanding on our brief preliminary report at a conference [31], we investigate the mode-selective frequency conversion in the OAM-compatible basis of LP_{11a} and LP_{11b} modes.

Hence, this paper presents the experimental investigation of nonlinear-optical signal processing in the FMF in the basis of LP_{11a} and LP_{11b} modes, which can be used to construct OAM_l modes with orbital angular momentum $l = \pm 1$: $OAM_{\pm 1} = (LP_{11a} \pm i\, LP_{11b})/2^{½}$. The experimental progress toward OAM-entangled photon-pair generation is described in Section 2.1. Section 2.2 reports the experimental demonstration of spatial-mode-selective frequency conversion in this mode basis. In both Sections 2.1 and 2.2, the demonstrations are performed with a classical signal. Section 3 presents the discussion and conclusions about this work.

2. Experimental Investigation of OAM-Compatible $\chi^{(3)}$ Nonlinear Processes for Spatially-Entangled State Generation and Spatial-Mode-Selective Frequency Conversion in FMF

The use of nonlinear-optical devices for spatially-multimode classical and quantum information processing was pioneered by the demonstration of noiseless image amplification by a spatially-broadband phase-sensitive optical parametric amplifier [32]. After this early experiment, theoretical understanding has been developed for spatially-broadband parametric amplification [33,34] and frequency conversion [35] in bulk-crystal media. The theory development culminated in the derivation of the spatial modes of such bulk devices [36–38], which undergo independent evolutions without coupling to one another. These modes, closely related to the Schmidt modes used in the analysis of spontaneous parametric down-conversion, are obtained by a singular-value decomposition of the Green's

function describing the light propagation in the crystal, which is a technique previously used to analyze the quantum noise of solitons in optical fiber [39–41]. The understanding of complex spatial interactions in the bulk nonlinear-optical devices has soon led to the proposals of image amplifiers [22,42] and mode-selective frequency converters [22] based on multimode waveguides in $\chi^{(2)}$ media. The latter have been subsequently experimentally demonstrated [23,24]. Given that FMFs provide great flexibility in mode- and dispersion-engineering, they are excellent candidates for achieving similar functionality in a $\chi^{(3)}$ nonlinear medium. Hence, we have demonstrated the spatial-mode-selective frequency conversion [25–30] and key processes for spatially-entangled photon-pair generation [16–19,30] in the LP_{01} and LP_{11} mode basis in the FMF. Below we extend this approach to OAM-compatible LP_{11a} and LP_{11b} mode basis. The intra- and inter-modal Kerr nonlinearities [43], Raman interactions [44], and a few-mode parametric amplification [45] in FMFs have also been studied recently.

As the nonlinear medium for the IM-FWM in all our experiments, we have chosen a graded-index elliptical-core FMF [12], to be referred to as three-mode fiber (TMF) below, which supports three non-degenerate spatial modes: LP_{01}, LP_{11a}, and LP_{11b}. The TMF's key parameters are as follows [12]: The optical loss is about 0.2 dB/km for all of the modes; the 10% core ellipticity breaks the LP_{11} mode degeneracy and keeps the distributed crosstalk between any two modes below –27 dB; the calculated effective areas of the LP_{01} and the $LP_{11a,b}$ modes are 89 μm^2 and 125 μm^2 at 1550 nm, respectively, resulting in a rather modest value of the nonlinear constant $\gamma_{01/11} = 0.7/W/km$ responsible for IM-FWM between LP_{01} and the LP_{11} modes and limiting the conversion efficiencies achievable with our available pump power.

2.1. Experiments Toward Generation of OAM-Entangled Photon Pairs

The spatial-mode entanglement scheme is realized by a combination of two IM-FWM processes, Processes 1 and 2, as shown in Figure 1a. The two employed IM-FWM processes are:

1. IM-FWM process 1: With the assistance of pump 1 in mode LP_{11a} and pump 2 in mode LP_{11b}, a signal photon is created in mode LP_{11a} at frequency ν_s, while the idler photon is created in the orthogonal mode LP_{11b} at frequency ν_i.
2. IM-FWM process 2: In the presence of pump 3 in mode LP_{11a} and pump 4 in mode LP_{11b}, a signal photon at frequency ν_s is created in mode LP_{11b}, whereas the idler photon is created in the orthogonal mode LP_{11a} at frequency ν_i.

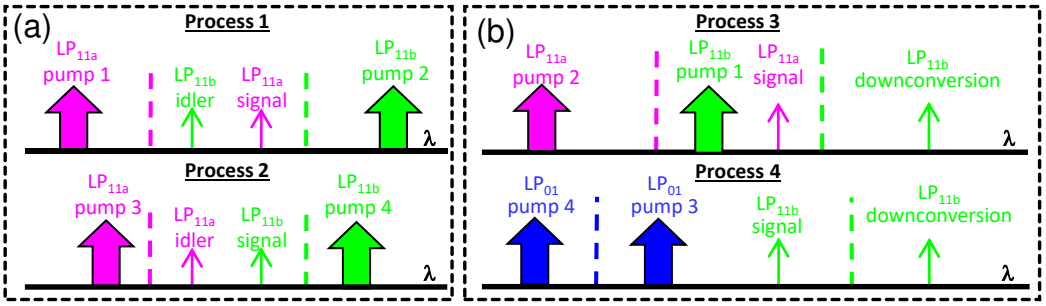

Figure 1. (**a**) Two parametric processes, whose combination enables OAM-entangled photon-pair generation in the TMF. (**b**) Two parametric processes, whose combination enables OAM-compatible mode-selective frequency conversion in the TMF. The colored dashed line represents the location of the wavelength representing the average frequency of the two waves belonging to the same spatial mode of that color.

With all four pumps present, processes 1 and 2 take place simultaneously. Their photon pair generation probabilities can be equalized by adjusting relative powers of the two pump pairs, which results in the generation of the maximally-entangled state $|\mathrm{LP_{11b}}\rangle_s |\mathrm{LP_{11a}}\rangle_i + e^{i\varphi} |\mathrm{LP_{11a}}\rangle_s |\mathrm{LP_{11b}}\rangle_i$, where phase φ can be changed by varying the phase difference $\Delta\varphi = (\varphi_{p1} + \varphi_{p2}) - (\varphi_{p3} + \varphi_{p4})$ between the two pairs of pumps. For $\varphi = \pi$, this state is equivalent to the OAM-entangled state $|l = +1\rangle_s |\ l = -1\rangle_i - |\ l = -1\rangle_s |\ l = +1\rangle_i$, where l is the orbital quantum number.

For each of the two processes in Figure 1a, both energy conservation and momentum conservation are required for the nonlinear interaction. Equation (1) describes the energy conservation relationship for the processes 1 and 2:

$$\begin{aligned} \nu_{p1} + \nu_{p2} &= \nu_s + \nu_i\,, \ \text{(Process 1)} \\ \nu_{p3} + \nu_{p4} &= \nu_s + \nu_i\,. \ \text{(Process 2)} \end{aligned} \tag{1}$$

Here, ν_{p1}, ν_{p2}, ν_{p3}, and ν_{p4} denote the frequencies of pumps 1, 2, 3, and 4, respectively. The momentum conservation is satisfied by the phase-matching condition for the four interacting waves. This condition for IM-FWM involving two spatial modes has been obtained in [10] and consists of two requirements:

1. The number of photons in each spatial mode should be preserved (i.e., if the signal and idler are in two different spatial modes, then one pump should be in the signal's spatial mode, and the other pump—in the idler's mode);
2. The group velocity at the average frequency of the two waves in one mode ($\mathrm{LP_{11a}}$ in our case) should be equal to the group velocity at the average frequency of the two waves in the other mode ($\mathrm{LP_{11b}}$ in our case).

These average frequencies, converted to wavelengths, are shown by the dashed lines in Figure 1a. Figure 2 shows measured relative inverse group velocities (RIGV) $1/v_g$ of $\mathrm{LP_{01}}$, $\mathrm{LP_{11a}}$, and $\mathrm{LP_{11b}}$ modes of our TMF. The curve of $\mathrm{LP_{11b}}$ is approximately parallel to the curve of $\mathrm{LP_{11a}}$ and is horizontally shifted by ~17 nm ($\Delta\nu_1$ = 2.1 THz), i.e., the phase-matching is satisfied when the dashed lines in Figure 1a are separated by 17 nm. This phase-matching condition [10] can be expressed as the following equation:

$$\begin{aligned} \tfrac{\nu_{p1}+\nu_s}{2} &= \tfrac{\nu_{p2}+\nu_i}{2} + \Delta\nu_1\ , \ \text{(Process 1)} \\ \tfrac{\nu_{p3}+\nu_i}{2} &= \tfrac{\nu_{p4}+\nu_s}{2} + \Delta\nu_1\ . \ \text{(Process 2)} \end{aligned} \tag{2}$$

Assuming known signal and idler frequencies, we can solve the system of Equations (1) and (2) for the four pump frequencies required for the OAM entanglement generation:

$$\begin{aligned} \nu_{p1} &= \nu_i + \Delta\nu_1, \\ \nu_{p2} &= \nu_s - \Delta\nu_1, \\ \nu_{p3} &= \nu_s + \Delta\nu_1, \\ \nu_{p4} &= \nu_i - \Delta\nu_1. \end{aligned} \tag{3}$$

Thus, the energy conservation (1) and momentum conservation (2) impose 4 constraints on the frequencies of the 6 involved waves, shown by Equation (3), and any two frequencies that are not separated by $\Delta\nu_1$ [i.e., are shown on different lines of Equation (3)] can be arbitrarily chosen. The remaining 4 frequencies are obtained from Equation (3).

In our experimental demonstration, the wavelengths of the signal and idler are chosen to be at 1564.8 nm and 1558.4 nm, respectively, which results in pumps 1, 2, 3, and 4 placed at 1541.3, 1582.4, 1547.3, and 1576.1 nm, respectively, as calculated by Equation (3). The experimental schematic is shown in Figure 3. The input signal and pumps (Ando AQ4321, Ando AQ8201-13E, and three Photonetics 3642 HE1550 tunable external cavity lasers) are

carved by intensity modulators (standard telecom 10 GHz modulators from JDSU, Covega, and Fujitsu) into 10-ns-long flat-top pulses with a 10-MHz repetition rate (10% duty cycle). The optical pulses are amplified by telecom-grade C- and L-band erbium-doped fiber amplifiers (EDFAs) and coupled from fiber to free space using three fiber collimators.

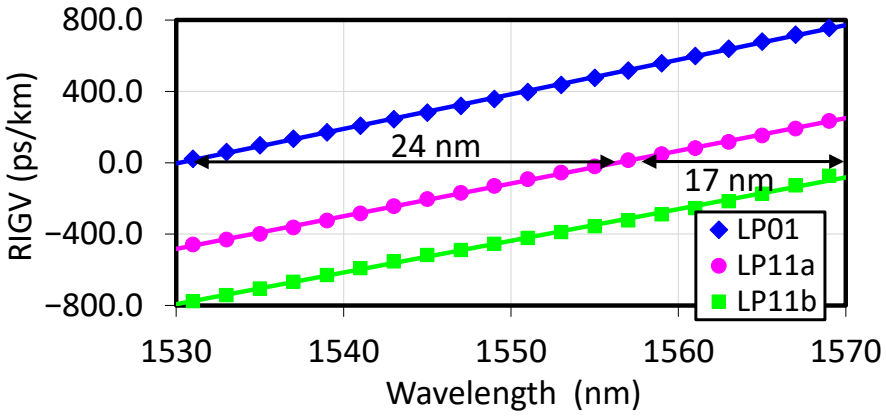

Figure 2. Measured relative inverse group velocity (RIGV) data for the modes of our TMF.

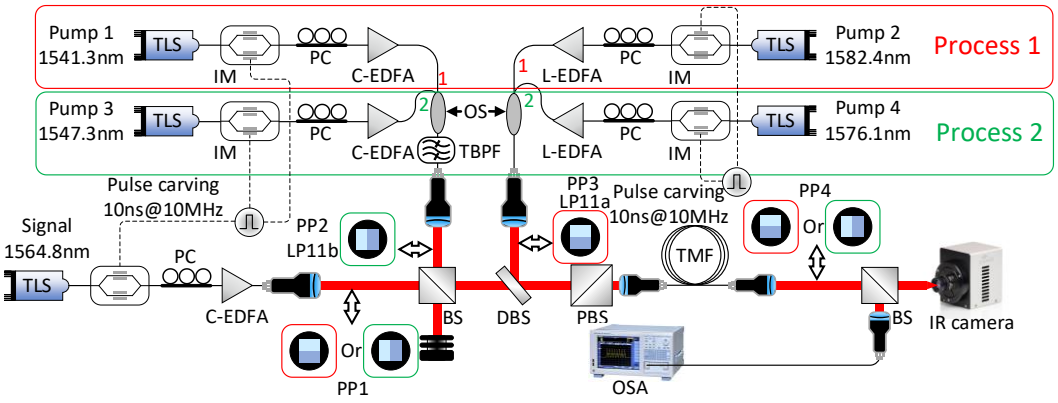

Figure 3. Experimental setup for investigation of OAM entanglement generation. TLS: tunable laser source; PC: polarization controller; C-EDFA: C-band erbium-doped fiber amplifier; L-EDFA: L-band erbium-doped fiber amplifier; TBPF: tunable optical bandpass filter; OS: optical switch; IM: intensity modulator; PP: phase plate; BS: beam splitter; DBS: dichroic beam splitter; PBS: polarizing beam splitter; TMF: three-mode fiber; OSA: optical spectrum analyzer; IR: infrared.

In process 1, signal and pump 1 are combined by a beam splitter (BS) in free space, and their spatial modes are individually converted to LP_{11a} by two corresponding phase plates (PPs), PP1 and PP2, respectively. One half of the glass-made PP is covered with a photoresist to introduce an additional π phase shift to the incident light wave, compared to the other half that is not covered by the photoresist. By placing the photoresist boundary at the center of the incident fundamental Gaussian beam (LP_{01} mode), we can convert it into LP_{11} mode. By rotating the PP, LP_{01} can be converted into LP_{11a}, $LP_{11b,}$ or a superposition of these two modes. Pump 2 is converted to LP_{11b} mode by a phase plate PP3 and combined with signal and pump 1 via a dichroic beam splitter (DBS). The three waves pass through a polarization beam splitter (PBS) to ensure their polarizations are aligned. After the PBS, the three waves are coupled into a 1-km-long TMF by a fiber collimator. The TMF output is coupled to free space by another fiber collimator, followed by a free-space BS, which sends half of the output light to an infrared camera, while the remaining half is coupled by a fiber collimator into a standard single-mode fiber (SSMF) connected to the optical spectrum analyzer (OSA). In this arrangement the OSA measures the LP_{01} mode output of the TMF, since only this mode can couple into the fundamental mode of the SSMF. By

inserting phase plate PP4 prior to the SSMF coupling, the LP_{11a} or LP_{11b} mode output of TMF can be converted into LP_{01} mode, with its spectrum observed on the OSA. Thus, the OSA can independently measure the LP_{01}, LP_{11a}, and LP_{11b} outputs (referred to as "output ports" below) of the TMF.

In this proof-of-concept experiment, we study the processes 1 and 2 separately. In process 2, pump 1 and pump 2 are replaced by pump 3 and pump 4, respectively, by an optical switch (OS). For this process, the signal's spatial mode is changed from LP_{11a} to LP_{11b} mode by rotating PP1 by 90°. To maximize IM-FWM, we co-polarize all three input waves entering the TMF. In future experiments, the OS will be replaced by wavelength multiplexers to enable the combination of processes 1 and 2 by the simultaneous presence of all 4 pumps.

We characterize the idler mode purity by comparing the idler power in the target spatial mode and the idler power in the undesired spatial mode of the TMF. Therefore, the purity of process 1 is calculated by the ratio of the power between the idler in LP_{11b} mode and the idler in LP_{11a} mode, and the mode purity for process 2 is calculated by the ratio of powers between the idler in LP_{11a} mode and the idler in LP_{11b} mode.

To show that these two parametric processes are only sensitive to a specific spatial mode of the signal, we measure their spatial-mode selectivity by comparing the idler power generated in the desired process (idler mode LP_{11b} with the input signal in the mode LP_{11a} for process 1, idler mode LP_{11a} with the input signal in the mode LP_{11b} for process 2) and the idler power in the desired mode, but generated in the undesirable process, i.e., with the input signal of the same power as before, but in the wrong mode (signal mode LP_{11b} for process 1, signal mode LP_{11a} for process 2).

Figure 4 shows the spectra at the LP_{11a} (blue traces) and LP_{11b} (magenta traces) output ports of the TMF for processes (a) 1 and (b) 2. The significant difference in the idler powers of the two traces indicates high spatial-mode purity of the idler, which is better than 22 dB for process 1 and better than 31 dB for process 2 (after subtracting the background amplified spontaneous emission noise). The average powers inside the TMF are 0 dBm for the signal in all cases and 15, 9.5, 17, and 7.5 dBm for pumps 1, 2, 3, and 4, respectively.

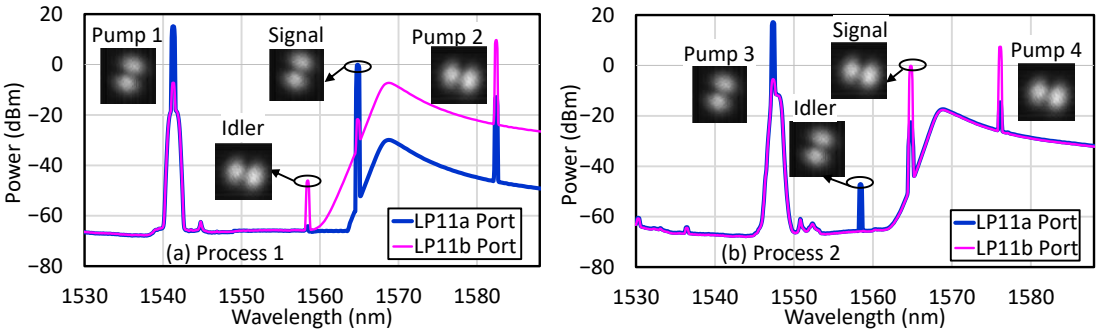

Figure 4. Optical spectra, measured at the LP_{11a} (blue traces) and LP_{11b} (magenta traces) output ports of the TMF for processes (**a**) 1 (signal in LP_{11a} mode) and (**b**) 2 (signal in LP_{11b} mode).

The easily measurable signal-to-idler classical conversion efficiency (CE, measured as the ratio of the output idler and input signal powers) is given by $CE = g - 1 = \langle n \rangle$, where g is the phase-insensitive parametric gain, and $\langle n \rangle$ is the average number of generated spontaneous parametric photons per mode, also representing the probability of a single spontaneous signal-idler photon pair generation for our case of CE << 1. In the perfectly phase-matched regime $CE = \sinh^2[2\gamma(P_{1(3)}P_{2(4)})^{1/2}L] \approx 4\gamma^2 P_{1(3)}P_{2(4)}L^2 << 1$, where L is the fiber length, $P_{i(j)}$ is the power of the pump with index $i = 1, 2$ (for process 1) or $j = 3, 4$ (for process 2), and $\gamma = n_2\omega/(cA_{\text{eff}})$ is the nonlinear constant, with A_{eff} being the effective area of the nonlinear interaction, equal to the inverse of the intensity overlap integral between

the modes LP_{11a} and LP_{11b}. We require CE = $\langle n \rangle$ << 1 to ensure that the probability of simultaneous generation of two pairs $\langle n \rangle^2$ is negligibly small.

In Figure 4, CEs are –46.0 dB and –47.0 dB for the processes 1 and 2, respectively. The CEs of the undesirable processes, separately measured by injecting the signal into the wrong mode (LP_{11b} for process 1 and LP_{11a} for process 2), are suppressed by more than 30.0 dB and 26.9 dB, compared to processes 1 and 2, respectively. This indicates high spatial-mode selectivity of our IM-FWM processes.

The presence of the TMF group velocity dispersion leads to gradual walk-off among the 4 interacting waves in each process. The largest group walk-off is between the signal and idler waves in process 1, which in our case amounts to ~430 ps at the end of the fiber. For 10-ns-long pump pulses used in our experiment, this is equivalent to a 4.3% reduction in the state fidelity (from 100% to 95.7%), which could be improved by using shorter fiber (custom-made highly nonlinear FMF) and higher pump power.

To summarize, we used a classical seed signal to experimentally verify the mode-selective properties of two IM-FWM parametric processes, in which a low-gain parametric amplifier in TMF couples the LP_{11a} signal to the LP_{11b} idler and the LP_{11b} signal to the LP_{11a} idler. In the spontaneous regime, the combination of these two processes with a particular relative phase difference $\Delta\varphi$ between the two pump pairs would generate OAM-entangled signal-idler photon pairs. We have demonstrated the conversion efficiencies of at least –47 dB with mode selectivity of about 27 dB or better, producing the idler beam with mode purity of 22 dB or better. The demonstrated CEs are high enough for practical applications and can be further increased to CE~1% (higher CEs than that are not desirable due to a noticeable two-pair generation probability) by raising the four pump powers while still keeping the total power below 1W. The next step will be to optimize the pump multiplexing scheme, both to minimize the losses and to stabilize the pump phase difference $\Delta\varphi$. Spontaneous regime would, in addition, require strong suppression of the amplified spontaneous emission of the pump beams at signal and idler frequencies, as well as narrow bandpass filtering of the output to minimize the contribution of the Raman noise [24]. It is worth noting that the IM-FWM process permits modal phase-matching of signal/idler and pumps separated by more than one Raman Stokes shift [14], which can potentially mitigate any noise effects from the parasitic Raman interactions.

2.2. Experiments on OAM-Compatible Spatial-Mode-Selective Frequency Conversion

The spatial-mode-selective frequency conversion is realized by a combination of two IM-FWM processes, shown in Figure 1b:

1. In the presence of pump 1 in mode LP_{11b} and pump 2 in mode $LP_{11a,}$ process 3 transfers the signal in mode LP_{11a} to a wavelength-converted beam in mode LP_{11b}.
2. In the presence of pumps 3 and 4 in mode $LP_{01,}$ process 4 transfers the signal in mode LP_{11b} to the same wavelength-converted beam in mode LP_{11b}.

When both processes occur simultaneously, any superposition of signal modes LP_{11a} and LP_{11b}, including the OAM modes $(LP_{11a} \pm i\, LP_{11b})/2^{1/2}$, can be selectively converted to the new frequency, while the orthogonal superposition is left untouched at the signal frequency. The relative mode weights in the selected superposition are chosen by the relative strengths of processes 3 and 4, which are, in turn, determined by the products of powers of pumps 1 and 2 (for process 3) and of pumps 3 and 4 (for process 4). The relative phase between the modes in the superposition is determined by the pump phase difference $\Delta\varphi = (\varphi_{p1} - \varphi_{p2}) - (\varphi_{p3} - \varphi_{p4})$. For example, $\Delta\varphi = \mp\pi/2$ selects the mode with OAM $l = \pm 1$. Note that, if both pumps in either process are identically phase-modulated to suppress stimulated Brillouin scattering, this modulation does not disturb the relative phase $\Delta\varphi$ and does not broaden the spectra of the signal and wavelength-converted beams.

By adjusting $\Delta\varphi$ and relative pump powers of processes 3 and 4, one can demultiplex any spatial mode from (LP_{11a}, LP_{11b}) mode space by converting it to a new wavelength. Unlike the linear-optics-based spatial-mode demultiplexers such as photonic lanterns or multi-plane light converters [46], this demultiplexer can be dynamically reconfigured to select another mode without introducing any extra loss in the signal path.

To calculate the phase-matching conditions for the processes 3 and 4, we need to use the horizontal shifts of ~17 nm ($\Delta\nu_1$ = 2.1 THz) between the RIGV curves for LP_{11a} and LP_{11b} modes and ~24 nm ($\Delta\nu_2$ = 3.0 THz) between the curves for LP_{01} and LP_{11a} modes in Figure 2. The energy conservation and phase-matching conditions (momentum conservation) are shown, respectively, by Equations (4) and (5) below:

$$\begin{aligned} \nu_{p1} + \nu_s &= \nu_{p2} + \nu_{\mathrm{WC}}, \quad \text{(Process 3)} \\ \nu_{p3} + \nu_s &= \nu_{p4} + \nu_{\mathrm{WC}}, \quad \text{(Process 4)} \end{aligned} \tag{4}$$

$$\begin{aligned} \tfrac{\nu_{p2}+\nu_s}{2} &= \tfrac{\nu_{p1}+\nu_{\mathrm{WC}}}{2} + \Delta\nu_1, \qquad \text{(Process 3)} \\ \tfrac{\nu_{p3}+\nu_{p4}}{2} &= \tfrac{\nu_s+\nu_{\mathrm{WC}}}{2} + \Delta\nu_1 + \Delta\nu_2. \text{ (Process 4)} \end{aligned} \tag{5}$$

Here, the subscript "WC" denotes the frequency of the wavelength-converted beam. From Equations (4) and (5), we can find 4 constraints on the frequencies of the 6 waves involved:

$$\begin{aligned} \nu_{\mathrm{WC}} &= \nu_s - \Delta\nu_1, \\ \nu_{p2} &= \nu_{p1} + \Delta\nu_1, \\ \nu_{p3} &= \nu_s + \Delta\nu_2, \\ \nu_{p4} &= \nu_s + \Delta\nu_1 + \Delta\nu_2. \end{aligned} \tag{6}$$

Here, two frequencies, ν_s (or ν_{p3}) and ν_{p1} (or ν_{p2}), can be arbitrarily chosen, whereas the frequencies of the four remaining waves are calculated from Equation (6).

In the experiment, the signal and converted-beam wavelengths are 1583.0 nm and 1601.1 nm, respectively, while the wavelengths of pumps 1, 2, 3, and 4 are 1558.3, 1541.1, 1560.1, and 1542.9 nm, respectively. Figure 5 shows the experimental setup for OAM-compatible spatial-mode-selective frequency conversion. All pumps and signals are carved into 10-ns-long flat-top pulses, and pumps are amplified with telecom-grade C-band EDFAs using an arrangement similar to that described in Section 2.1. Pump 2 is converted to LP_{11a} mode by a phase plate PP1, combined with the signal in free space by a dichroic beam splitter DBS, and then combined with LP_{01}-mode pumps 3 and 4 by a free-space beam-splitter BS1. Pump 1 is converted to LP_{11b} mode by a phase plate PP2, combined with these 4 beams by BS2, and coupled into the 1-km-long TMF by a collimator preceded by a PBS. The TMF output is coupled to the free space via a fiber collimator and is split between an infrared camera and another fiber collimator that is connected to the optical spectrum analyzer OSA by SSMF. In this arrangement, the OSA measures the spectrum of the LP_{01} mode at the TMF output (the only mode that couples to the SSMF). We will refer to this as the measurement at "the LP_{01} output port" of the TMF. By inserting a phase plate PP4 or PP5 prior to the SSMF collimator, we can convert LP_{11a} or LP_{11b} mode, respectively, to the SSMF mode. That way, we can select any output mode ("output port") of the TMF to be measured by the OSA. The spatial mode of the signal can be gradually varied from LP_{11a} to LP_{11b} by rotating the phase plate PP3 (when it is at 0°, it generates 100% LP_{11a} mode, and when it is at 90°, it generates 100% LP_{11b} mode; in the intermediate positions, it generates various two-mode superpositions). To maximize IM-FWM, we co-polarize all three input waves in each process with the help of the PBS.

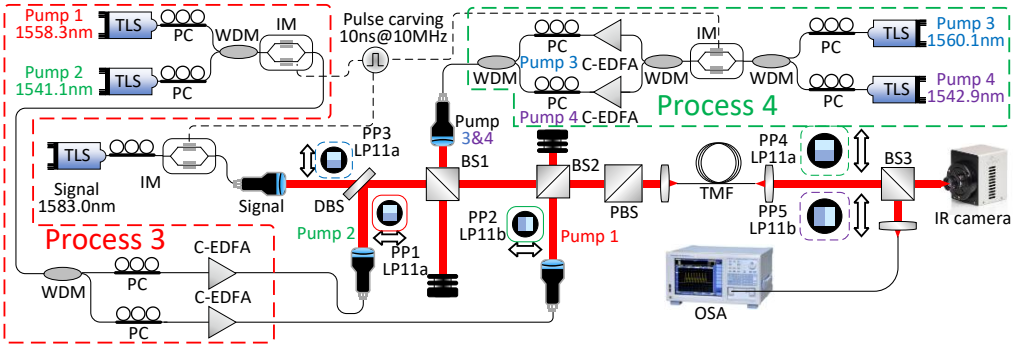

Figure 5. Experimental setup for OAM-compatible spatial-mode-selective frequency conversion. TLS: tunable laser source; PC: polarization controller; WDM: wavelength-division multiplexer; C-EDFA: C-band erbium-doped fiber amplifier; IM: intensity modulator; PP: phase plate; BS: beam splitter; DBS: dichroic beam splitter; PBS: polarizing beam splitter; TMF: three-mode fiber; OSA: optical spectrum analyzer; IR: infrared.

The mode selectivity of each individual process is quantified by comparing the conversion efficiency (CE) for the "desired" signal mode (LP_{11a} in process 3, LP_{11b} in process 4) to the CE for the "undesirable" signal mode (LP_{11b} in process 3, LP_{11a} in process 4). The gray and blue traces in Figure 6 show the ratio of these two efficiencies (inverted crosstalk) for process 3 to be 23.8 dB (after subtracting the background amplified spontaneous emission noise). Inverted crosstalk for process 4 is 29.2 dB, as shown in Figure 7a. The "desired" CEs are –43.2 dB and –43.1 dB for the processes 3 and 4, respectively. The mode purity of the converted beam can be quantified by the ratio between its powers measured at the correct (LP_{11b}) and wrong (LP_{11a}) output ports [only the correct output port LP_{11b} is shown in Figures 6 and 7a], which is 31.1 dB for process 3 and 27.3 dB for process 4.

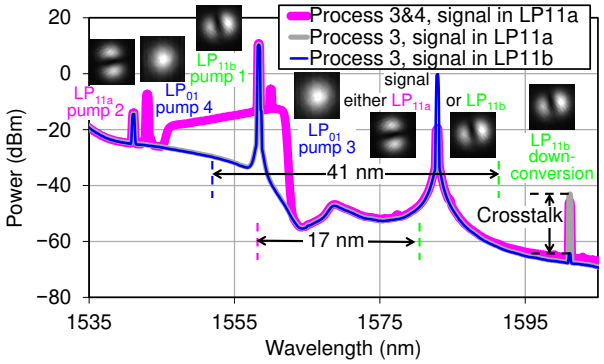

Figure 6. Spectra at the LP_{11b} output port for process 3 alone (gray, blue) and processes 3 and 4 combined (magenta).

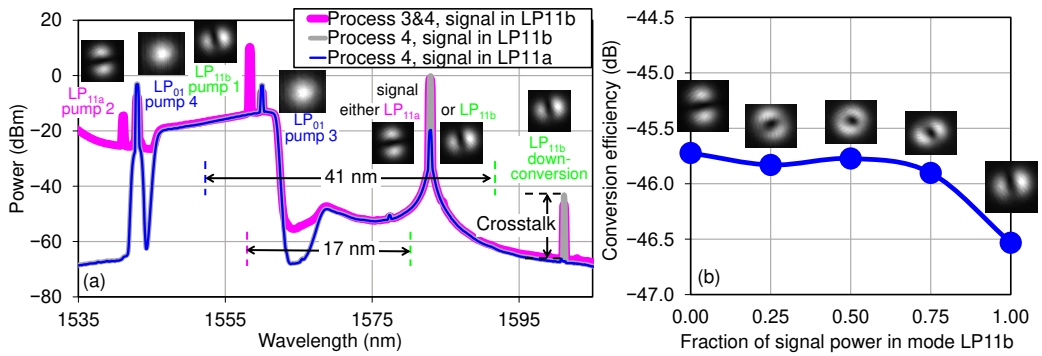

Figure 7. (**a**) Spectra at the LP_{11b} output port for process 4 alone (gray, blue) and processes 3 and 4 combined (magenta). (**b**) Conversion efficiencies (CEs) for various signal mode superpositions.

Figures 6 and 7a also show the spectra of the LP_{11b} output port for processes 3 and 4 taking place simultaneously (i.e., when all 4 pumps are present) by the magenta traces. Average powers inside the TMF are 0 dBm for the signal and 10.5, 5.5, 9, and 7 dBm for pumps 1, 2, 3, and 4, respectively. At these powers, the CEs for processes 3 and 4 are nearly equal. If we had stable phase $\Delta\varphi = (\varphi_{p1} - \varphi_{p2}) - (\varphi_{p3} - \varphi_{p4})$, we would have been able to select for wavelength conversion a superposition of LP_{11a} and LP_{11b} signal modes with a specific relative phase, e.g., an OAM mode. Since the phase $\Delta\varphi$ is also responsible for the direction of $\omega_{p1} + \omega_{p4} = \omega_{p2} + \omega_{p3}$ phase-sensitive parametric amplification process among the 4 pumps (this process may require coupling a small fraction of pump 1 into the LP_{11a} mode to meet the IM-FWM selection rules), it can be stabilized with a single phase-locking loop by monitoring one of the pump waves. However, such stabilization, typically relying on mutually coherent pumps derived from an optical frequency comb, is out of the scope for this paper, and our $\Delta\varphi$ fluctuates randomly on a 0.1–1 μs scale. This means that we can observe mode-independent wavelength conversion of the signal, as both LP_{11a} and LP_{11b} components of any signal superposition are independently converted to LP_{11b} mode at the new frequency and then added incoherently. This is illustrated in Figure 7b, which shows nearly the same CEs (within a 0.8 dB range from one another), measured for various signal superpositions with a weight of the LP_{11b} component ranging from 0 to 100%.

To summarize, we have proposed and experimentally implemented two simultaneous IM-FWM processes enabling OAM-compatible mode-selective frequency conversion. We have achieved the mode-selective wavelength conversion efficiencies of about –43 dB with better than –23 dB crosstalk for modes LP_{11a} and LP_{11b}. For various superpositions of these modes, the results show that, in the absence of the pump phase stabilization, our scheme produces mode-independent signal frequency conversion in OAM-compatible (LP_{11a}, LP_{11b}) mode space. Since the data symbol duration should be longer than the larger of the intra-modal and inter-modal group delays between the original and converted signals (335 ps in our case), the use of a shorter FMF with higher nonlinearity is desirable for future optical communication applications. Such a customized, highly nonlinear FMF with a reduced core size, along with a high-power EDFA used for the pumps, would also help to increase the CEs to practically important levels.

3. Discussion and Conclusions

This work extends the nonlinear-optical signal processing to classical and quantum communication applications involving OAM modes. It employs IM-FWM processes in few-mode fibers, which enable both spatial-mode and wavelength selectivity in wavelength converters and parametric photon-pair generators. These features are important for increasing the capacity of both classical and quantum communication links by employing multiple OAM spatial modes.

For the OAM-entangled photon-pair generation, we have designed and experimentally demonstrated with a classical seed signal two mode-selective IM-FWM processes that couple signal and idler photons in the orthogonal modes of the OAM-compatible (LP_{11a}, LP_{11b}) mode space. We have measured the conversion efficiencies of at least -47 dB with high mode selectivity of about 27 dB or better, producing the idler beam with mode purity of 22 dB or better. At our pulse repetition rate, this corresponds to a ~200 pairs per second generation rate for the spontaneous (unseeded) regime.

For the mode-selective wavelength conversion, we have designed and experimentally demonstrated a combination of two simultaneous mode-selective IM-FWM processes that can potentially selectively wavelength-convert any signal mode superposition in the OAM-compatible (LP_{11a}, LP_{11b}) mode space without perturbing the orthogonal mode su-

perposition. For each process separately, we have achieved the mode-selective wavelength conversion efficiency of about −43 dB with low crosstalk of less than −23 dB. For both processes running simultaneously, in the absence of active stabilization of the pump phase, we have achieved mode-independent signal frequency conversion in the OAM-compatible (LP_{11a}, LP_{11b}) mode space. The mode-selective wavelength conversion can be used for projective measurements at the receiver side of quantum communication links, as well as for spatial-mode de-multiplexing in classical communication systems and networks. In the latter case, in contrast to wavelength conversion in conventional highly-nonlinear fibers, IM-FWM in FMF uses modal phase-matching and does not require operation in the vicinity of zero-dispersion wavelength, which mitigates inter-channel nonlinearities (four-wave mixing, cross-phase modulation) that are otherwise capable of degrading the performance of WDM communication systems.

In the future work, the key relative phase between the pump pairs needs to be stabilized, and the loss in pump multiplexing arrangement needs to be reduced. The former can be achieved by deriving the pump waves from different components of an optical frequency comb and controlling one of their phases by a relatively slow feedback loop driven by a particular IM-FWM product among the pumps. The use of a frequency comb generated either electro-optically or nonlinear-optically [47] would eliminate the issues with frequency stability and linewidths of 4 independent pump lasers, which could otherwise require a complex combination of frequency-locking and fast phase-locking loops. The spatial mode multiplexing of the pumps can be facilitated by either a photonic lantern with low insertion loss and high crosstalk or a multi-plane light conversion [46] with higher insertion loss and lower crosstalk, depending on the overall loss budget of the system.

Author Contributions: M.V.: concept; M.V. and X.L.: overall architecture and methodology; A.S. and C.G.: experimental setup design and measurements; F.P.: three-mode fiber and its dispersion characterization; C.G. and A.S.: writing the first draft; C.G., A.S. and M.V.: preparing the figures; M.V.; project supervision; all authors: review and editing of the manuscript. All authors have read and agreed to the published version of the manuscript.

Funding: This work has been supported in part by the National Science Foundation grants ECCS-1937860, ECCS-1842680, and OMA-2231388.

Data Availability Statement: The data that support the findings of this study are available from the corresponding author upon reasonable request.

Conflicts of Interest: The authors declare no conflicts of interest.

References

1. Puttnam, B.J.; Rademacher, G.; Luís, R.S. Space-division multiplexing for optical fiber communications. *Optica* **2021**, *8*, 1186–1203. [CrossRef]
2. Xavier, G.B.; Lima, G. Quantum information processing with space-division multiplexing optical fibres. *Commun. Phys.* **2020**, *3*, 9. [CrossRef]
3. Bittermann, J.A.; Bulla, L.; Ecker, S.; Neumann, S.P.; Fink, M.; Bohmann, M.; Friis, N.; Huber, M.; Ursin, R. Photonic entanglement during a zero-g flight. *Quantum* **2024**, *8*, 1256. [CrossRef]
4. Rübeling, P.; Heine, J.; Johanning, R.; Kues, M. Quantum and coherent signal transmission on a single-frequency channel via the electro-optic serrodyne technique. *Sci. Adv.* **2024**, *10*, eadn8907. [CrossRef]
5. Chang, K.C.; Cheng, X.; Sarihan, M.C.; Vinod, A.K.; Lee, Y.S.; Zhong, T.; Gong, Y.X.; Xie, Z.; Shapiro, J.H.; Wong, F.N.; et al. 648 Hilbert-space dimensionality in a biphoton frequency comb: Entanglement of formation and Schmidt mode decomposition. *npj Quan. Inf.* **2021**, *7*, 48. [CrossRef]
6. Chang, K.C.; Sarihan, M.C.; Cheng, X.; Zhang, Z.; Wong, C.W. Large-alphabet time-bin quantum key distribution and Einstein–Podolsky–Rosen steering via dispersive optics. *Quan. Sci. Technol.* **2024**, *9*, 015018. [CrossRef]
7. Löffler, W.; Euser, T.G.; Eliel, E.R.; Scharrer, M.; Russell, P.S.J.; Woerdman, J.P. Fiber transport of spatially entangled photons. *Phys. Rev. Lett.* **2011**, *106*, 240505. [CrossRef]

8. Kang, Y.; Ko, J.; Lee, S.M.; Choi, S.K.; Kim, B.Y.; Park, H.S. Measurement of the entanglement between photonic spatial modes in optical fibers. *Phys. Rev. Lett.* **2012**, *109*, 020502. [CrossRef]
9. Cozzolino, D.; Polino, E.; Valeri, M.; Carvacho, G.; Bacco, D.; Spagnolo, N.; Oxenløwe, L.K.K.; Sciarrino, F. Air-core fiber distribution of hybrid vector vortex-polarization entangled states. *Adv. Photonics* **2019**, *1*, 046005. [CrossRef]
10. Essiambre, R.J.; Mestre, M.A.; Ryf, R.; Gnauck, A.H.; Tkach, R.W.; Chraplyvy, A.R.; Sun, Y.; Jiang, X.; Lingle, R. Experimental investigation of inter-modal four-wave mixing in few-mode fibers. *IEEE Photonics Technol. Lett.* **2013**, *25*, 539–542. [CrossRef]
11. Anjum, O.F.; Guasoni, M.; Horak, P.; Jung, Y.; Petropoulos, P.; Richardson, D.J.; Parmigiani, F. Polarization-insensitive four-wave-mixing-based wavelength conversion in few-mode optical fibers. *J. Light. Technol.* **2018**, *36*, 3678–3683. [CrossRef]
12. Parmigiani, F.; Horak, P.; Jung, Y.; Grüner-Nielsen, L.; Geisler, T.; Petropoulos, P.; Richardson, D.J. All-optical mode and wavelength converter based on parametric processes in a three-mode fiber. *Opt. Express* **2017**, *25*, 33602–33609. [CrossRef]
13. Anjum, O.F.; Guasoni, M.; Horak, P.; Jung, Y.; Suzuki, M.; Hasegawa, T.; Bottrill, K.; Richardson, D.J.; Parmigiani, F.; Petropoulos, P. Selective wavelength conversion in a few-mode fiber. *Opt. Express* **2019**, *27*, 24072–24081. [CrossRef] [PubMed]
14. Rottwitt, K.; Koefoed, J.G.; Christensen, E.N. Photon-pair sources based on intermodal four-wave mixing in few-mode fibers. *Fibers* **2018**, *6*, 32. [CrossRef]
15. Guo, C.; Su, J.; Zhang, Z.; Cui, L.; Li, X. Generation of telecom-band correlated photon pairs in different spatial modes using few-mode fibers. *Opt. Lett.* **2019**, *44*, 235–238. [CrossRef]
16. Li, X.; Cui, L.; Guo, X.; Ou, Z.Y.; Vasilyev, M. Fiber-based sources of quantum light for quantum information processing. In Proceedings of the Asia Communications and Photonics Conference (ACP), Shanghai, China, 24–27 October 2021. paper M4A.1.
17. Shamsshooli, A.; Guo, C.; Parmigiani, F.; Li, X.; Vasilyev, M. Toward generation of spatially-entangled photon pairs in a few-mode fiber. In Proceedings of the Conference on Lasers and Electro-Optics (CLEO), Washington DC, USA, 10–15 May 2020. paper JTh2A.27.
18. Shamsshooli, A.; Guo, C.; Parmigiani, F.; Li, X.; Vasilyev, M. Progress Toward Generation of Spatially-Entangled Photon Pairs in a Few-Mode Fiber. In Proceedings of the IEEE Photonics Conference (IPC), Vancouver, BC, Canada, 28 September–1 October 2020. paper MI2.2.
19. Shamsshooli, A.; Guo, C.; Parmigiani, F.; Li, X.; Vasilyev, M. Progress Toward Spatially-Entangled Photon-Pair Generation in a Few-Mode Fiber. *IEEE Photonics Technol. Lett.* **2021**, *33*, 864–867. [CrossRef]
20. Shamsshooli, A.; Guo, C.; Parmigiani, F.; Li, X.; Vasilyev, M. Toward generation of orbital-angular-momentum-entangled photon pairs in a few-mode fiber. In Proceedings of the Frontiers in Optics conference, Washington DC, USA, 14–17 September 2020. paper FM1D.2.
21. Shibahara, K.; Mizuno, T.; Ono, H.; Nakajima, K.; Miyamoto, Y. Long-haul DMD-unmanaged 6-mode-multiplexed transmission employing cyclic mode-group permutation. In Proceedings of the Optical Fiber Communication (OFC) conference, San Diego, CA, USA, 8–12 March 2020. paper Th3H.3.
22. Kwon, Y.B.; Vasilyev, M. Mode-selective frequency up-conversion in a χ(2) waveguide. *Proc. SPIE* **2014**, *8964*, 89640N.
23. Kwon, Y.B.; Giribabu, M.; Li, L.; Samudrala, S.C.; Langrock, C.; Fejer, M.M.; Vasilyev, M. Experimental demonstration of spatial-mode-selective frequency up-conversion in a multimode χ(2) waveguide. In Proceedings of the Conference on Lasers and Electro-Optics (CLEO), San Jose, CA, USA, 5–10 June 2016. paper STh3P.4.
24. Kwon, Y.B.; Giribabu, M.; Langrock, C.; Fejer, M.M.; Vasilyev, M. Single-photon-level spatial-mode-selective frequency up-conversion in a multimode χ(2) waveguide. In Proceedings of the Conference on Lasers and Electro-Optics (CLEO), San Jose, CA, USA, 14–19 May 2017. paper FF2E.1.
25. Shamsshooli, A.; Guo, C.; Parmigiani, F.; Li, X.; Vasilyev, M. Mode-Selective Frequency Conversion in a Three-Mode Fiber. In Proceedings of the Conference on Lasers and Electro-Optics (CLEO), San Jose, CA, USA, 10–15 May 2020. paper SM3P.3.
26. Shamsshooli, A.; Guo, C.; Vasilyev, M.; Parmigiani, F.; Li, X. Reconfigurable mode-selective frequency conversion in a three-mode fiber. In Proceedings of the IEEE Photonics Conference (IPC), Vancouver, BC, Canada, 28 September–1 October 2020. paper ThF1.2.
27. Shamsshooli, A.; Guo, C.; Parmigiani, F.; Li, X.; Vasilyev, M. Reconfigurable Spatial-Mode-Selective Frequency Conversion in a Three-Mode Fiber. *IEEE Photonics Technol. Lett.* **2021**, *33*, 860–863. [CrossRef]
28. Shamsshooli, A.; Kwon, Y.B.; Guo, C.; Parmigiani, F.; Li, X.; Langrock, C.; Fejer, M.M.; Vasilyev, M. Spatial-Mode-Selective Frequency Conversion. In Proceedings of the Photonics in Switching and Computing Conference, Washington, DC, USA, 27–29 September 2021. paper Tu4A.1.
29. Shamsshooli, A.; Guo, C.; Vasilyev, M.; Parmigiani, F.; Li, X.; Akasaka, Y.; Palacharla, P. Emerging applications of wavelength conversion. In Proceedings of the IEEE Photonics Conference (IPC), Vancouver, BC, Canada, 17–21 October 2021. paper ThE2.1.
30. Shamsshooli, A.; Kwon, Y.B.; Guo, C.; Vasilyev, M. Devices for quantum communication over mode-division-multiplexing systems. *Proc. SPIE* **2023**, *12446*, 124460E.
31. Shamsshooli, A.; Guo, C.; Parmigiani, F.; Li, X.; Vasilyev, M. Toward OAM-selective frequency conversion in a three-mode fiber. In Proceedings of the Conference on Lasers and Electro-Optics (CLEO), San Jose, CA, USA, 11–13 May 2021. paper SM1F.5.

32. Choi, S.-K.; Vasilyev, M.; Kumar, P. Noiseless Optical Amplification of Images. *Phys. Rev. Lett.* **1999**, *83*, 1938–1941, Erratum in *Phys. Rev. Lett.* **2000**, *84*, 1361. [CrossRef]
33. Vasilyev, M.; Stelmakh, N.; Kumar, P. Phase-sensitive image amplification with elliptical Gaussian pump. *Opt. Express* **2009**, *17*, 11415–11425. [CrossRef] [PubMed]
34. Vasilyev, M.; Stelmakh, N.; Kumar, P. Estimation of the spatial bandwidth of an optical parametric amplifier with plane-wave pump. *J. Mod. Opt.* **2009**, *56*, 2029–2033. [CrossRef]
35. Vasilyev, M.; Kumar, P. Frequency up-conversion of quantum images. *Opt. Express* **2012**, *20*, 6644–6656. [CrossRef] [PubMed]
36. Vasilyev, M.; Annamalai, M.; Stelmakh, N.; Kumar, P. Quantum properties of a spatially-broadband traveling-wave phase-sensitive optical parametric amplifier. *J. Mod. Opt.* **2010**, *57*, 1908–1915. [CrossRef]
37. Annamalai, M.; Stelmakh, N.; Vasilyev, M.; Kumar, P. Spatial modes of phase-sensitive parametric image amplifiers with circular and elliptical Gaussian pumps. *Opt. Express* **2011**, *19*, 26710–26724. [CrossRef]
38. Annamalai, M.; Stelmakh, N.; Kumar, P.; Vasilyev, M. Compact representation of the spatial modes of a phase-sensitive image amplifier. *Opt. Express* **2013**, *21*, 28134–28153. [CrossRef]
39. Levandovsky, D.; Vasilyev, M.; Kumar, P. Perturbation theory of quantum solitons: Continuum evolution and optimum squeezing by spectral filtering. *Opt. Lett.* **1999**, *24*, 43–45. [CrossRef]
40. Levandovsky, D.; Vasilyev, M.; Kumar, P. Soliton squeezing in a highly transmissive nonlinear optical loop mirror. *Opt. Lett.* **1999**, *24*, 89–91, Erratum in *Opt. Lett.* **1999**, *24*, 423. [CrossRef]
41. Levandovsky, D. Quantum Noise Suppression in Optical Fibers. Ph.D. Thesis, Northwestern University, Evanston, IL, USA, 1999.
42. Annamalai, M.; Vasilyev, M. Phase-sensitive multimode parametric amplification in a parabolic-index waveguide. *IEEE Photonics Technol. Lett.* **2012**, *24*, 1949–1952. [CrossRef]
43. Cui, L.; Liu, X.; Guo, C.; Zhang, Z.; Zhao, N.; Vasilyev, M.; Li, X. Measurement of effective nonlinear coefficients in few-mode fibers. *Opt. Lett.* **2019**, *44*, 5768–5771. [CrossRef]
44. Zhang, Z.; Cheng, H.; Guo, C.; Cui, L.; Zhang, Y.; Mo, Q.; Yu, H.; Vasilyev, M.; Li, X. Investigation of Spontaneous Raman Scattering in Few-Mode Fibers: Dependence on Polarization and Spatial Modes. *J. Light. Technol.* **2021**, *39*, 6281–6287. [CrossRef]
45. Huo, N.; Cheng, H.; Zhu, S.; Guo, C.; Zhang, Y.; Mo, Q.; Cui, L.; Vasilyev, M.; Li, X. Gain-equalizable few-mode fiber optical parametric amplifier in telecom band. *Opt. Comm.* **2022**, *508*, 127735. [CrossRef]
46. Fontaine, N.K.; Ryf, R.; Chen, H.; Neilson, D.; Carpenter, J. Design of high order mode-multiplexers using multiplane light conversion. In Proceedings of the European Conference on Optical Communications (ECOC), Gothenburg, Sweden, 17–21 September 2017.
47. Ataie, V.; Myslivets, E.; Kuo, B.P.-P.; Alic, N.; Radic, S. Spectrally Equalized Frequency Comb Generation in Multistage Parametric Mixer With Nonlinear Pulse Shaping. *J. Light. Technol.* **2014**, *32*, 840–846. [CrossRef]